

# The Surface Tension and Density of Molten $\text{Sc}_2\text{O}_3$ , $\text{La}_2\text{O}_3$ , $\text{Y}_2\text{O}_3$ , $\text{Al}_2\text{O}_3$ , and $\text{MgO}$ Measured *via* a Pendant Droplet Method



JONATHAN PARAS, OSAMU TAKEDA, MINDY WU, and ANTOINE ALLANORE

A thermal imaging furnace (TIF) was used to study the physical properties of molten  $\text{Sc}_2\text{O}_3$ ,  $\text{La}_2\text{O}_3$ ,  $\text{Y}_2\text{O}_3$ ,  $\text{Al}_2\text{O}_3$  and  $\text{MgO}$  *via* a containerless method. The density and surface tension of molten droplets of  $\text{Sc}_2\text{O}_3$ ,  $\text{La}_2\text{O}_3$ ,  $\text{Y}_2\text{O}_3$ ,  $\text{Al}_2\text{O}_3$ , and  $\text{MgO}$  suspended from their own solid were measured *in situ* using live video under a range of oxygen partial pressures ( $1 \rightarrow 10^{-6}$  atm  $\text{O}_2$ ). To the best knowledge of the authors, this is the first time the surface tension and density of molten  $\text{MgO}$  and  $\text{Sc}_2\text{O}_3$  have been reported. A relationship between molten oxide surface tension and the enthalpy of vaporization is proposed, and a comparison is drawn between the oxide properties and similar relationships previously established for liquid metals.

<https://doi.org/10.1007/s11663-022-02508-3>  
© The Author(s) 2022

## I. INTRODUCTION

THE surface tension is the energy required to extend a surface which is at equilibrium with its gas phase by a unit area under constant temperature, pressure, and composition. In the absence of other forces, surface tension causes a droplet of material to become spherical in order to minimize the area of exposed surface. However, most materials processes occur under the force of gravity, whose magnitude depends on a material's density. Additionally, materials processes often occur with multiple phases in close contact. The design of liquid-state processes must, therefore, consider how the surface tension and density of liquids vary as a function of process parameters such as temperature and composition.

Examples of such processes include the interaction of liquid metals with oxide slags during furnace tapping, casting, and welding.<sup>[1-4]</sup> Relative differences in the density of the materials in these multiphase processes determine the mixing of metals and oxides during

furnace tapping, and their surface tension can determine the wettability of the metal and oxide melts to a weldment or the walls of a casting crucible.<sup>[1,5,6]</sup> While the surface tension and density are readily available for pure metals, the same is not true for alloys, salts, or oxides, and these values are often of particular importance for industry. Because many processes occur either in air or are otherwise at risk of oxygen contamination, significant effort has been put forth to understand and engineer the physical properties of the relevant molten oxides that are either formed or employed during liquid-state processing.<sup>[3,7,8]</sup> This article will, therefore, focus on the surface tension and density of molten oxides.

Modeling of the surface tension of multicomponent oxides come in two forms: thermodynamic and pseudo-empirical. As detailed in Lupis, the first attempt to quantify the thermodynamic origin of the surface tension comes from Gibbs who demonstrated that one can treat the surface as its own phase with which the gas (or relevant phase in the case of general interfacial tension) and the bulk material are in equilibrium.<sup>[9,10]</sup> The interface would then differentially contribute to the system's internal energy as follows:

$$dE = \sigma dA, \quad [1]$$

where  $dA$  is the change in the size of the interface and  $\sigma$  the surface tension. This treatment was later expanded upon to include multicomponent systems and was related by Butler and others to the system Gibbs energy of mixing in alloys and oxides as follows<sup>[11-13,15]</sup>:

JONATHAN PARAS, MINDY WU, and ANTOINE ALLANORE are with the Department of Materials Science and Engineering, MIT, 77 Massachusetts Ave, Cambridge, MA 02139. Contact e-mail: allanore@mit.edu OSAMU TAKEDA is with the Department of Metallurgy, Graduate School of Engineering, Tohoku University, 6-6-02 Aramaki, Aoba-ku, Sendai 980-8579, Japan.

Manuscript submitted October 12, 2021; accepted March 23, 2022.

$$\begin{aligned}
\sigma &= \sigma_A + \frac{RT}{A_A} \ln \left( \frac{1 - N_B^S}{1 - N_B^B} \right) \\
&+ \frac{1}{A_A} \overline{G}_A^{E,S}(T, N_B^S) - \frac{1}{A_A} \overline{G}_A^{E,B}(T, N_B^B) \\
&= \sigma_B + \frac{RT}{A_B} \ln \left( \frac{N_B^S}{N_B^B} \right) + \frac{1}{A_B} \overline{G}_B^{E,S}(T, N_B^S) \\
&- \frac{1}{A_B} \overline{G}_B^{E,B}(T, N_B^B),
\end{aligned} \tag{2}$$

where  $A_x$  is the molar surface area of the pure species  $x$  (related to the density),  $\sigma_x$  is the pure species surface tension,  $N_x^S$  and  $N_x^B$  are the surface and bulk concentration of a particular species, and  $\overline{G}_x^{E,S}$  and  $\overline{G}_x^{E,B}$  are the partial molar surface and bulk excess Gibbs energies, respectively. This method allows for the estimation of the surface tension of a solution if there exists supporting solution thermodynamic data and the pure member surface tensions are known. Pseudo-empirical methods as outlined by Mills *et al.* typically employ a weighting of the end-member properties using empirical (and often chemistry-specific) coefficients to estimate the solution surface tension.<sup>[8,16]</sup> Using either the thermodynamic or pseudo-empirical frameworks to estimate surface tension requires knowledge of the end-member surface tensions and densities.

Work by Tanaka and colleagues demonstrated the utility of Eq. [2] in evaluating the surface tension of binary alloy mixtures but noted significant inadequacies in using this approach to describe the surface tension of multicomponent oxide and ionic liquids.<sup>[17,18]</sup>

Modeling of the density has proven more difficult than the surface tension; there do not exist equations that describe the molar volume of mixing of molten solutions in any general capacity.<sup>[3]</sup> However, as pointed out in the Slag Atlas, generalized Vegard's law rules serve as an approximation for the density of a system across the composition space, so long as the melt does not exhibit strong network forming or short-range ordering propensities.<sup>[19]</sup> For specific chemistries, additivity rules for the density may be expressed as the sum of an additivity factor for each constituent element. It can be demonstrated that the density of a solution is related to the end-member densities and excess molar volumes as follows:

$$\rho = \sum_x \rho_x \frac{V_x}{\sum_x V_x^o + \sum_x \overline{V}_x^E} \tag{3}$$

where  $\rho_x$  are the end-member densities,  $V_x^o$  the end-member molar volumes, and  $\overline{V}_x^E$  the excess partial molar volumes. The excess partial molar volume can then be related to the change in the activity coefficients with respect to pressure as follows:

$$\overline{V}_x^E = RT \frac{\partial \ln(\gamma_x)}{\partial P}, \tag{4}$$

where here,  $\gamma_x$  refers to the activity coefficient.

A priori knowledge of the surface tension and density of pure oxide melts is, therefore, necessary to estimate the surface tension and density of molten oxide solutions. Such estimation ability is particularly important for metallurgical slags which can contain up to 10 different metals in solution, making experimental exploration time consuming and expensive.<sup>[3]</sup>

There is still considerable spread across surface tension and density measurements even for well-explored compounds such as  $\text{Al}_2\text{O}_3$ . This can be attributed to the experimental difficulties associated with the temperature and reactivity of the melts. Oxides melt at high temperature (often  $>2000$  °C) increasing the risk of contamination with crucible materials. The surface tension itself is sensitive to small changes in composition, magnifying the effect of contamination.<sup>[20]</sup> Calculation of the surface tension from droplet measurement techniques often require the liquid-state density.<sup>[21]</sup>

Significant effort has, therefore, been expended developing techniques to study the surface tension and density of oxides using sessile drop, archimedean, falling drop, maximum bubble pressure, and the meniscus methods.<sup>[22-27]</sup> Unfortunately, they all require the melt to be in contact with some form of foreign material, ensuring some degree of contamination and implicitly limiting the range of chemistries and temperatures that can be studied. This work proposes to measure the surface tension and density of some molten oxides using a containerless pendant droplet method to overcome some of the aforementioned challenges.

The surface tension and density are readily available for many pure molten metals but comparatively little is known about molten oxides outside commonly used compounds like  $\text{Al}_2\text{O}_3$ .<sup>[22-33]</sup> Few surface tension and density measurements of rare-earth oxides such as  $\text{La}_2\text{O}_3$ , and  $\text{Y}_2\text{O}_3$  have been made despite their use tuning slag properties in steel casting and solar grade silicon processing.<sup>[30,34-36]</sup> No such measurements beyond the melting point have been reported for molten  $\text{Sc}_2\text{O}_3$  which range between 2300 °C and 2489 °C.<sup>[37-42]</sup> Otherwise, measurements of physical properties such as the density (3.83 g cm<sup>-3</sup><sup>[43-49]</sup>) and thermal expansion coefficient ( $8.854 \times 10^{-6}$  K<sup>-1</sup><sup>[50]</sup>) have been confined to the solid. The densities of chemically similar rare-earth sesquioxides, such as  $\text{Y}_2\text{O}_3$  and  $\text{Yb}_2\text{O}_3$ , have been measured and range from 4.5 to 8 g cm<sup>-3</sup> at melting.<sup>[36]</sup> Highly reactive alkaline earth-molten oxides like MgO also lack reported surface tension and density values near the melting point despite its ubiquitous use in slags.<sup>[51]</sup> We will, therefore, focus on  $\text{Al}_2\text{O}_3$ ,  $\text{Y}_2\text{O}_3$ ,  $\text{La}_2\text{O}_3$ ,  $\text{Sc}_2\text{O}_3$ , and MgO as model oxide compounds that provide a mix of well-studied systems and highly reactive melts without prior measurements. Success in this endeavor will allow us to validate the utility of the proposed approach and support the future estimation of the surface tension in systems that contain molten oxides of  $\text{Sc}_2\text{O}_3$  and MgO.

## II. METHODS

### A. Setup

It is difficult to prevent contamination or partial melting of most refractory-crucible materials at temperatures sufficient to melt most oxides ( $>2000\text{ }^{\circ}\text{C}$ ). Therefore, a containerless method for the measurement of the density, surface tension, and melting temperature was sought. Nakanishi and Wu *et al.* previously demonstrated that a thermal imaging furnace (TIF) could be used to stabilize and observe molten droplets suspended from their own solid rod at nominally unbounded temperatures.<sup>[52,53]</sup> The advantage of this method over typical pendant droplets is that the droplet is not vertically suspended from within a crucible of differing material, but rather itself. This reduces the possibility of droplet contamination. A thermal imaging furnace was, therefore, used in this study.

The TIF was a Crystal Systems Corporation Model TX-12000-I-MIT-VPO-PC as seen in Figure 1. The furnace consisted of 4 Xenon lamps. Each 3 kW lamp was positioned within an ellipsoidal mirror. The geometric arrangement of the lamps enabled the focal point

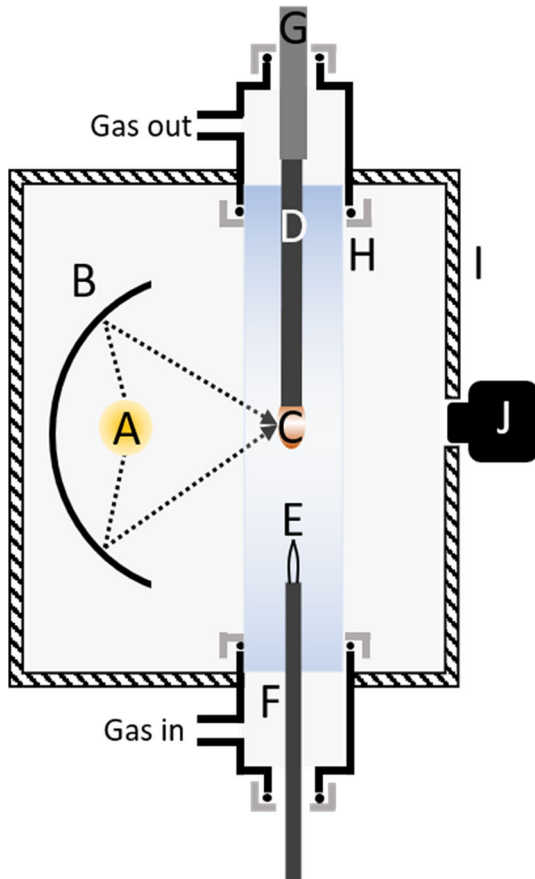


Fig. 1—Schematic of a thermal imaging furnace from a quarter view of the furnace. There are three additional xenon lamps at 90 degree angles around the centerline. The labeled regions are (A) Xenon arc lamp. (B) Ellipsoidal focusing mirror. (C) Hot zone. (D) Sample rod. (E) Type C thermocouple. (F) Supporting sheath for thermocouple (alumina). (G) Mo sample holder (H) Quartz tube. (I) Steel casing.

of the mirrors to coincide with the centerline of the system in a region hereafter called the “hot zone.” This four-lamp setup also ensures that the azimuthal temperature gradient is  $< 50\text{ }^{\circ}\text{C}$  and that the hot zone covers an estimated region of the centerline which is 1 mm in height. The effective size of the hot zone can vary depending on the sample emissivity and size. The maximum temperature gradient outside the hot zone and the droplet moving along the centerline was estimated to be  $200\text{ }^{\circ}\text{C mm}^{-1}$ .

Sample rods were suspended in the hot zone using two methods. The first coupled the rod to an upper rotating shaft using a hollow molybdenum cylinder with set screws which were used to hold the solid oxide rod directly. For irregularly shaped samples, Ni wire (99.9 pct pure) was wrapped around the top of the oxide rod and was connected to a hook which hung from a stainless steel upper rotating shaft. Either assembly could be lowered such that the end of the oxide rod was positioned inside the hot zone of the furnace. A type C thermocouple was used to measure the temperature.

The thermocouple was introduced from the bottom of the setup and raised into contact with the sample. The upper and lower assemblies were controlled using stepper motors with submillimeter precision and were sealed entirely inside of a quartz tube (Technical Glass Products Inc.). The interior of the quartz tube was purged 3 times and backfilled with argon gas (Airgas Inc., UHP Ar  $> 99.999$  pct) before any experiments were conducted. During purge cycles, the quartz tube was evacuated to approximately 1325 Pa. A digital mass flow controller (Tylan General Inc., FC-260V) was used to establish argon flow at a rate of  $200\text{ mL min}^{-1}$  in the tube during experimentation.

Observation of the sample *in situ* was conducted by a panel mounted video camera and a Canon Rebel T5i DSLR mounted at portholes with line-of-sight to the hot zone.

### B. Melting Point of $\text{Sc}_2\text{O}_3$

The melting point of  $\text{Sc}_2\text{O}_3$  was measured by inserting a type C (W-Re) thermocouple into the molten droplet, then allowing the droplet to solidify around the thermocouple. The droplet was re-melted and allowed to cool. The melting temperature was attributed to the observed thermal arrest in the measured temperature profile and simultaneous visualization of the solidification event.

The temperatures observed in this study were outside the standard type C range ( $0\text{ }^{\circ}\text{C}$  to  $2320\text{ }^{\circ}\text{C}$ ). Thermocouple voltages were recorded using an Omega OMB-DAQ-55 at a frequency of 5.988 Hz. This voltage was converted to temperature values using previously measured temperature-voltage standards provided by Omega in Reference 54 for W-5Re/W-25Re wire. A best-fit curve of temperature vs thermocouple voltage was made, and the calculated temperature relied on a small extrapolation beyond the calibrated range of temperatures.

### C. Density

Density of the liquid state is difficult to measure using Archimedean principles because of the reactivity of oxide melts and lack of suitable crucible materials at relevant temperatures. Density was measured by quenching the droplets sufficiently quickly to create a vitrified molten region that could be cut and ground from the unmelted portion of the rod. This would then be weighed to provide the mass of the molten droplet at the observed temperature before quenching. A correction was made when cutting away the molten region. As indicated in Figure 2 for the correction of molten alumina, a trapezoidal unmelted region consistently formed in the quenched droplets. The unmelted part in the boundary between the molten droplet and solid rod was measured using image analysis and the volume of the unmelted region at high temperature was calculated using the thermal expansion coefficient. The volume and mass of the unmelted region were, therefore, subtracted to calculate the true melt density.

Axisymmetric sample generation was a priority. The volume of the molten droplet was computed by integrating their surface profile as an object of revolution as observed during the experiment. The liquid density was calculated by dividing the measured mass of the vitrified region of the sample by this computed volume.

### D. Surface Tension

Surface tension was measured by using a pendant droplet method.<sup>[53]</sup> Under gravity and its own capillarity, a suspended droplet assumes a shape dictated by the surface tension and density of the liquid. Long rods of the material were made such that the rod tip could be lowered into the hot zone to create a stable droplet. The

suspension of a molten droplet in Figure 3 (left) was imaged using a Canon Rebel T5i DSLR and post-processed in Mathematica (Figure 3 (right)).

The surface tension of  $\text{Sc}_2\text{O}_3$  was calculated using OpenDrop, a freely available software which numerically integrated the droplet profile to calculate the surface tension.<sup>[55]</sup> Error associated with the fitting process is described in more detail in Reference 55. The droplet was assumed to obey the Young–Laplace equation:

$$\sigma \left( \frac{1}{R_1} + \frac{1}{R_2} \right) = \Delta P := \Delta P_o - \Delta \rho g z, \quad [5]$$

where  $R_1$  and  $R_2$  are the principle radii of curvature,  $\Delta P$  is the Laplace pressure across the interface,  $\sigma$  is the surface tension,  $\Delta \rho$  is the difference between the droplet phase density and the continuous phase density



Fig. 3—(Left) Image of a molten  $\text{Sc}_2\text{O}_3$  droplet in the floating zone furnace. (Right) Image processed using Mathematica to produce an outline of the droplet surface.

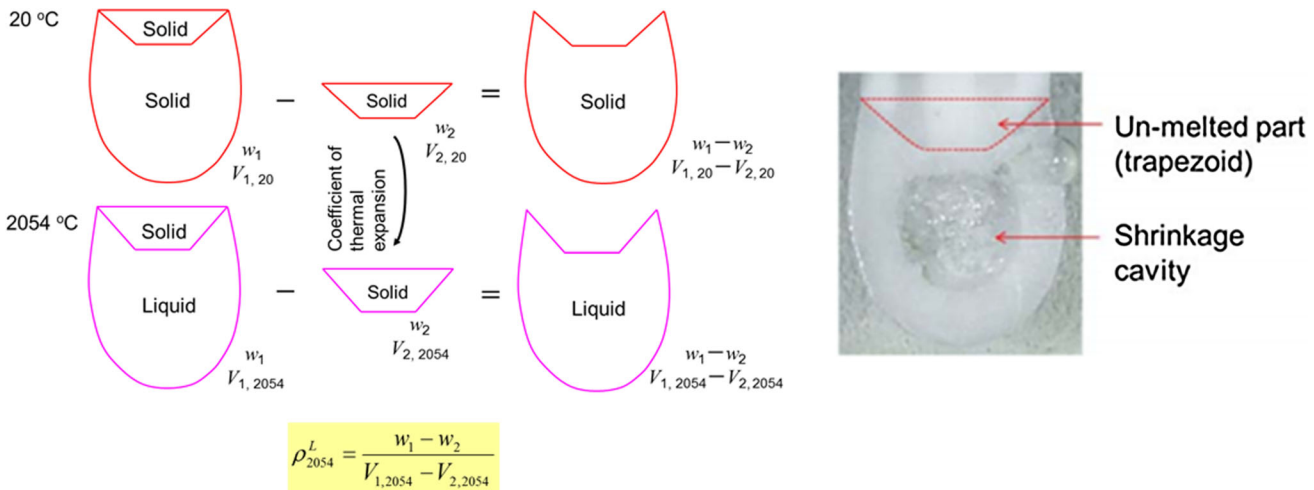


Fig. 2—Cross section of a solidified  $\text{Al}_2\text{O}_3$  droplet melted under argon (R) along with the scheme to correct for the true measured density (L). Note the contrast between the unmelted region and the rest of the droplet.

(in this case, the surrounding gas). OpenDrop handled the computationally difficult task of back-calculating the surface tension which produces the best fit of the observed droplet profile for  $\text{Sc}_2\text{O}_3$ .

The surface tension of  $\text{MgO}$ ,  $\text{Al}_2\text{O}_3$ ,  $\text{Y}_2\text{O}_3$ , and  $\text{La}_2\text{O}_3$  were calculated using the method proposed by Fordham *et al.*, who presented an analytical solution to the droplet shape based upon the Young-Laplace equation.<sup>[21]</sup>

### E. Pyrometry

Infrared temperature sensing was used during surface tension measurements to avoid disturbing the droplet and maintain sample purity while capturing images to measure its surface profile. An iR2<sup>TM</sup> Omega Pyrometer was used to measure radiative light between 0.8 and 1.7  $\mu\text{m}$  to calculate the temperature of the droplet based upon its emissivity. The pyrometer was used in single color mode in this case. The sensing area of the pyrometer was estimated to be between 10 and 20 mm in diameter.

Emissivity,  $\varepsilon$ , for  $\text{Sc}_2\text{O}_3$  in the liquid state as a function of temperature was unknown. Because of the background radiation from the xenon lamps, high reflection from the ellipsoidal mirrors, the emissivity was treated as a sensitivity setting when computing the temperature from the pyrometer for all surface tension and density measurements of  $\text{Sc}_2\text{O}_3$ . Future reference of  $\varepsilon$  will refer to this sensitivity parameter rather than the true emissivity of molten  $\text{Sc}_2\text{O}_3$ .

The pyrometer was calibrated by measuring two different  $\text{Sc}_2\text{O}_3$  rods of different  $\phi$  (9 mm and 4 mm in diameter) at identical lamp power (65 pct). Both samples produced identical temperature measurements as a function of the chosen  $\varepsilon$ . A type C thermocouple was inserted into one of the two samples, and the recorded temperature was used to find the appropriate emissivity such that the temperature value measured by the pyrometer was identical. This emissivity was found to be 0.371 at 2965 °C. The temperature values for the surface tension and density measurements of  $\text{Sc}_2\text{O}_3$  were measured using optical pyrometry.

### F. Sample Preparation

$\text{Sc}_2\text{O}_3$  powder of 99.95 pct purity was graciously provided by the Harima Refinery of Sumitomo Metal Mining Co. Impurities (wt pct) included Carbon (0.017), Hydrogen (0.0179), and Sulfur (<0.001) as determined through LECO analysis by Massachusetts Materials Research, Inc. This analysis implied that oxygen content was slightly lower than expected for this compound (34.2 vs expected 34.8 wt pct). Particle sizes of the powder were bimodally distributed and ranged from 8 to 170  $\mu\text{m}$ .

$\text{MgO}$  rods were cut out from a boat purchased from TEP. Co (99.9 pct purity).  $\text{Al}_2\text{O}_3$ ,  $\text{La}_2\text{O}_3$ , and  $\text{Y}_2\text{O}_3$  were commercially purchased (99.5 pct purity Alfa Aesar).

The powder was loaded into 260Q Diamond Clear latex balloons that were previously rinsed with ethanol to remove talc powder on the balloon interior. These balloons were then sealed and immersed in room-temperature oil and isostatically pressed to 172.4 MPa. The samples were then sintered in air for 12 hours at 1500 °C. Samples were heated at 4 °C  $\text{min}^{-1}$  from room temperature to 800 °C and 2 °C  $\text{min}^{-1}$  from 800 °C to 1500 °C. The ramp-down cycle was identical to the ramp up. Samples were sintered for such extended durations to ensure that even long rods that extended outside the hot zone of the furnace (CM Inc High-Temperature Tube Furnace) sintered adequately. Densities >95 pct were achieved. Final rod dimensions averaged 4 to 6 mm in diameter at a length of 5 cm.

## III. RESULTS AND DISCUSSION

### A. Surface Tension and Density of $\text{Al}_2\text{O}_3$

The surface tension and density of molten aluminum oxide were measured near the melting point under both ultra-high-purity argon and a pure oxygen atmosphere. These results are displayed in Table I. Both the density and surface tension did not significantly vary as a

**Table I. Density and Surface Tension as a Function of  $\text{pO}_2$  and Temperature for Various Molten Oxides**

Material	Temperature (K)	Surface Tension ( $\text{mN m}^{-1}$ )	Density ( $\text{g cm}^{-3}$ )	$\text{pO}_2$ (atm)
$\text{Al}_2\text{O}_3$	mp	$673 \pm 17$	$2.934 \pm 0.015$	$10^{-6}$ (UHP Ar)
		$675 \pm 16$	$2.948 \pm 0.057$	$10^0$
$\text{Sc}_2\text{O}_3$	3053	$739.1 \pm 66.8$	$3.32 \pm 0.13$	$10^{-6}$ (UHP Ar)
	3175	$765.7 \pm 7.02$	$3.05 \pm 0.03$	
	3190	$697.3 \pm 13.1$	$2.92 \pm 0.02$	
$\text{Y}_2\text{O}_3$	mp	$687 \pm 20$	$4.135 \pm 0.109$	$10^{-6}$ (UHP Ar)
		$725 \pm 6.4$	$4.122 \pm 0.150$	$10^{-3}$
		$740 \pm 15$	$4.153 \pm 0.049$	$10^0$
$\text{La}_2\text{O}_3$	mp	$547.8 \pm 16$	$5.275 \pm 0.164$	$10^{-6}$
		$556 \pm 18$	$5.248 \pm 0.155$	$10^{-3}$
		$572.5 \pm 27$	$5.236 \pm 0.133$	$10^0$
$\text{MgO}$	mp	$713 \pm 14$	$2.43 \pm 0.1$	$10^{0.55}$

mp: melting point.

function of oxygen partial pressure. Table II contains measurements of molten  $\text{Al}_2\text{O}_3$  density near the melting point from other works.

The results in Table II indicate that our method for measuring the molten state density is in general agreement with most authors except Zubarev *et al.* This anomalously low value for the density of molten alumina, as opined in Ikemiya *et al.*, can largely be attributed to interaction between the alumina and graphite substrate in the chosen sessile drop geometry.

Table III compares surface tension measurements across the literature with this work. Our value compares favorably with Kingery and Maurakh *et al.*'s work. Wartenberg *et al.* suffer from a lower surface tension largely because of a smaller molten density used in their calculations ( $2.5 \text{ g cm}^{-3}$ ).

In Rasmussen *et al.*'s work, a contact angle method was used in which molten  $\text{Al}_2\text{O}_3$  formed a meniscus within Mo and W capsules. They derived surface tension of 360 and 638  $\text{mN m}^{-1}$  in Mo and W capsules, respectively. It was noted in their work that

contamination with the substrate was an issue, even with apparent insolubility of the substrate material with molten  $\text{Al}_2\text{O}_3$ . Rasmussen's experiments also demonstrate that contamination can occur in pendant droplet geometries that utilize a sleeve material to create their droplet, which we avoid entirely by melting the tip of the material of interest from its own solid rod.

In addition, capsule experiments typically utilize X-rays to image the droplet, significantly impacting the accuracy of the measured droplet profile compared to the optical measurements conducted in our study. Zubarev *et al.*'s measurement encounters issues with interaction with the graphite substrate, calling their results into question. Most sessile drop measurements, as pointed out by Kingery, are not effective for molten oxides as they typically wet many inert substrates.<sup>[22]</sup>

Lihmann *et al.* reported a significant variation of the surface tension with atmospheric conditions contrary to what we observed. These results are displayed in Figure 4 along with our experimental data. It is not clear why He gas would decrease the surface tension. He and H cannot reduce  $\text{Al}_2\text{O}_3$  but the absorption of these atoms on the molten surface could potentially result in the observed reduction of the surface tension. Such an effect would disappear with sufficient superheating of the melt.

Ultimately our approach for measuring the surface tension and density agrees with the literature and provides strong validation for the utility of the proposed method in the exploration of other molten oxides.

## B. Melting Point, Density, and Surface Tension of $\text{Sc}_2\text{O}_3$

A plot of the temperature computed directly from the voltage as a function of time is presented in Figure 5. The melting point of  $\text{Sc}_2\text{O}_3$  was measured to be  $2362 \pm 47 \text{ }^\circ\text{C}$ . The melting point was calculated by estimating the onset of a thermal arrest upon cooling from a temperature above melting. This temperature was initially found by steadily increasing the lamp power while observing the droplet directly. Error in the

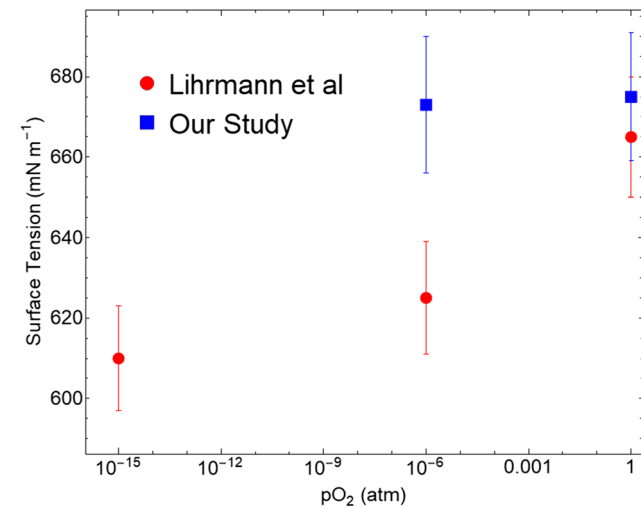


Fig. 4—A plot of the variation of surface tension with partial pressure of oxygen of molten  $\text{Al}_2\text{O}_3$ . Standard deviation of 3 experiments is given as the error bar.

**Table II. Literature Values of the Density of Molten  $\text{Al}_2\text{O}_3$  Near the Melting Point**

References	Method	Atmosphere	Density ( $\text{g cm}^{-3}$ )
Kingery <sup>[22]</sup>	SD	He	$2.97 \pm 0.05$
Kirshenbaum <sup>[23]</sup>	Arch	Ar	3.053
Maurakh <sup>[24]</sup>	FD	Ar	3.05
Zubarev <sup>[25]</sup>	SD	unknown	2.69
Mitin <sup>[28]</sup>	arch	Ar	3.04
Elyutin <sup>[26]</sup>	MBP	He	3.03
Rasmussen <sup>[27]</sup>	menis.	vacuum	3.01
Ikemiya <sup>[29]</sup>	MBP	Ar-10 pct $\text{H}_2$	$3.06 \pm 0.03$
This study	PD	Ar	$2.93 \pm 0.02$
		$\text{O}_2$	$2.95 \pm 0.06$

SD: Sessile drop, Arch: Archimedeal, FD: Falling drop, MBP: Maximum bubble pressure, Menis: Meniscus, PD: Pendant Drop.

**Table III. Surface Tension Measurements of Molten  $\text{Al}_2\text{O}_3$  Near Melting**

References	Method	Atmosphere	$\gamma$ ( $\text{mN m}^{-1}$ )
Wartenberg <sup>[30]</sup>	DW	vacuum	$580 \pm 30$
Kingery <sup>[22]</sup>	PD	He	$690 \pm 20$
Bartlett <sup>[31]</sup>	DW	unknown	551
Maurakh <sup>[24]</sup>	PD	Ar	680
	DW	Ar	670
McNally <sup>[32]</sup>	DW	Ar	600
Elyutin <sup>[26]</sup>	MBP	He	570
Rasmussen <sup>[27]</sup>	menis (Mo)	vacuum	$360 \pm 40$
	menis (W)		$638 \pm 100$
	PD		$574 \pm 68$
Lihmann <sup>[33]</sup>	PD	air	$665 \pm 1$
		He	$625 \pm 14$
		He-10 pct $\text{H}_2$	$610 \pm 13$
Ikemiya <sup>[29]</sup>	MBP	Ar-10 pct $\text{H}_2$	$606 \pm 6$
This Study	PD	Ar	$673 \pm 17$
		$\text{O}_2$	$675 \pm 16$

DW: Drop weight, PD: Pendant Drop, SD: Sessile Drop, Menis: Meniscus, MBP: Maximum Bubble Pressure, DC: Dipping Cylinder.

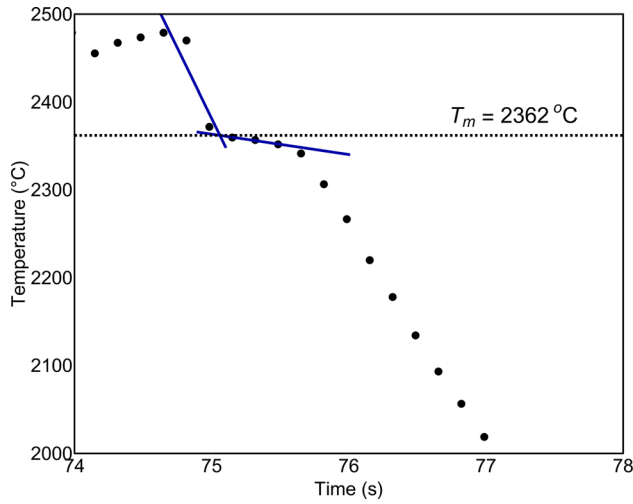


Fig. 5—Temperature vs duration of thermocouple insertion in molten  $\text{Sc}_2\text{O}_3$ . Lamps were extinguished at the peak-reported temperature value and the observed thermal arrest was used to evaluate the melting point.

temperature measurement (quoted by the equipment provider as  $\pm 2$  pct at these conditions) exceeded the difference in melting temperature for any arbitrary point chosen along the thermal arrest itself.

$\text{Sc}_2\text{O}_3$  melting temperatures have reportedly ranged from 2300 °C to 2489 °C.<sup>[37–42]</sup> Our value lies inside of the range of reported temperatures, with the most recently collected data (Shpilrain and Coutures *et al.*) clustered at the high end. The thermocouple tip itself may act as a heat sink, resulting in an underestimate of the melting temperature. Additionally, some degree of undercooling is expected for the thermal arrest. Such experimental difficulties have cast doubt on most results across the Sc-O system in addition to the melting point of  $\text{Sc}_2\text{O}_3$ .<sup>[56]</sup>

Density and surface tension variation with temperature are depicted in Figures 6 and 7. The density of  $\text{Sc}_2\text{O}_3$  varied between 3.32 and 2.92  $\text{g cm}^{-3}$ . Surface tension varied between 765 and 697  $\text{mN m}^{-1}$ . Measurements were conducted between temperatures ranging from 2780 °C to 2920 °C.

To the best knowledge of the authors, there do not exist reported values for the surface tension and density of molten  $\text{Sc}_2\text{O}_3$ . Of the rare-earth sesquioxides,  $\text{Sc}_2\text{O}_3$  has the one of the lowest solid densities at room temperature (3.85  $\text{g cm}^{-3}$ <sup>[43]</sup>), and this is reflected in its relatively smaller molten density in comparison to  $\text{La}_2\text{O}_3$  and  $\text{Sm}_2\text{O}_3$  as outlined in Table IV. For reference, a study of molten density and surface tension found for pure liquid Sc a density of 2.68  $\text{g cm}^{-3}$  and a surface tension of 939  $\text{mN m}^{-1}$  at melting.<sup>[57]</sup>

### C. Surface Tension and Density of $\text{Y}_2\text{O}_3$ and $\text{La}_2\text{O}_3$

The surface tension and density of molten  $\text{Y}_2\text{O}_3$  near the melting point and under argon were measured to be 687  $\text{mN m}^{-1}$  and 4.135  $\text{g cm}^{-3}$  respectively. The surface tension and density of molten  $\text{La}_2\text{O}_3$  near the melting

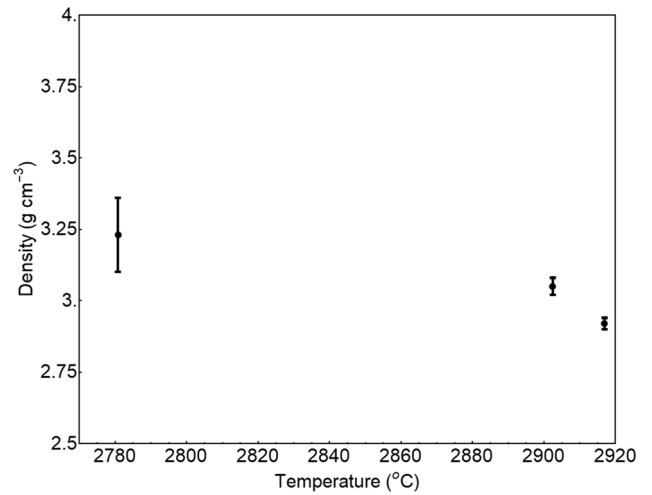


Fig. 6—Density of molten  $\text{Sc}_2\text{O}_3$  as a function of temperature. The error bar is the standard deviation from multiple experiments.

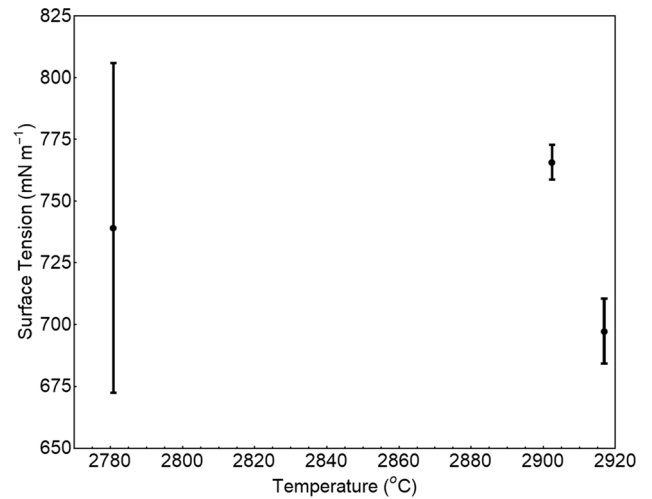


Fig. 7—The surface tension of molten  $\text{Sc}_2\text{O}_3$  as a function of temperature. The error bars are the standard deviation from multiple experiments.

**Table IV. Comparison of this Work's  $\text{Sc}_2\text{O}_3$  Surface Tension and Density With Various Sesquioxide Literature Values<sup>[29]</sup>**

Material	Density ( $\text{g cm}^{-3}$ )	$\gamma$ $\text{mN m}^{-1}$	Temperature (K)
$\text{Sc}_2\text{O}_3$	3.23	739	3053
$\text{La}_2\text{O}_3$	6.5	560	2573
$\text{Al}_2\text{O}_3$	2.99	599	2340
$\text{Ti}_2\text{O}_3$	3.83	580	2173
$\text{Sm}_2\text{O}_3$	6.8	815	2593

point and under argon were measured to be 548  $\text{mN m}^{-1}$  and 5.275  $\text{g cm}^{-3}$ . Little literature data exist on the surface tension and density of either. Wartenberg studied  $\text{La}_2\text{O}_3$  under vacuum using the drop weight method and found the density of  $\text{La}_2\text{O}_3$  was 6.5  $\text{g cm}^{-3}$  and the surface tension to be  $560 \pm 30$   $\text{mN m}^{-1}$ , which

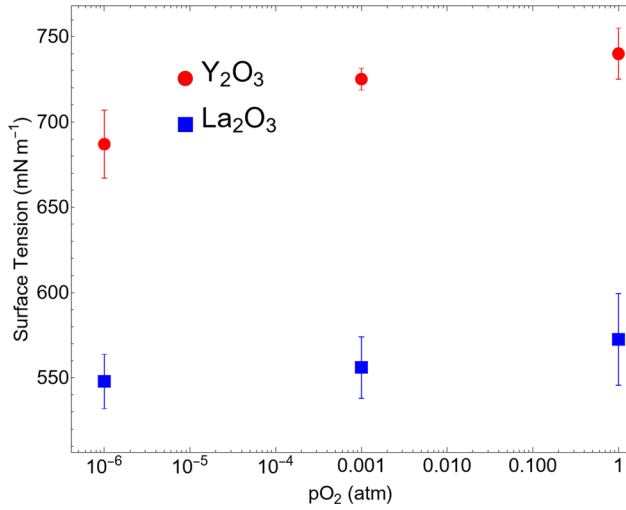


Fig. 8—Surface tension plotted against partial pressure of oxygen for La<sub>2</sub>O<sub>3</sub> and Y<sub>2</sub>O<sub>3</sub> samples. Standard deviation of four experiments is given as the error bar.

is within the range of our reported surface tension, although the difference in our density measurements calls into question the validity of their computed surface tension.<sup>[30]</sup>

Granier and Heurtrault measured the density at melting for both La<sub>2</sub>O<sub>3</sub> and Y<sub>2</sub>O<sub>3</sub> and found them to be 5.10 and 4.42 g cm<sup>-3</sup>, respectively, in better agreement with our experimental findings.<sup>[36]</sup> Additional data on La<sub>2</sub>O<sub>3</sub> and other molten oxides is summarized in Table IV from Ikemiya *et al.*<sup>[29]</sup>

The density did not exhibit a strong dependence on oxygen partial pressure in either material. As expected, the surface tension did. Figure 8 demonstrates the dependence of the surface tension on oxygen partial pressure for Y<sub>2</sub>O<sub>3</sub> and La<sub>2</sub>O<sub>3</sub>.

This may account for the discrepancy between the result reported by Wartenberg and our work, as their tests were conducted under vacuum. Lower oxygen partial pressure decreases the surface tension, while a larger density, all else being equal, should increase it. Therefore, it is postulated that these errors may be offsetting and explain the substantial agreement between our result and the Wartenberg experiment in spite of dissimilar molten densities.

The large error in the La<sub>2</sub>O<sub>3</sub> surface tension values is due to the oxide's relatively high density compared to its surface tension. This represents the chief limit of this technique; it is difficult to stabilize molten droplets for high-density materials with lower surface tensions.

#### D. Surface Tension and Density of MgO

The surface tension and density of MgO were  $713 \pm 14$  mN m<sup>-1</sup> and 2.43 g cm<sup>-3</sup>, respectively. The error is the standard deviation from four experiments. It was difficult to stabilize a MgO droplet in argon or under vacuum. Pure O<sub>2</sub> up to 3.5 atm was used for the measurement. To the best knowledge of the authors, surface tension and density measurements for MgO

Table V. Compilation of the Surface Tension of Various Metallic and Metalloid Elements<sup>[65]</sup>

Material	$T_m$ (K)	$\sigma$ mN m <sup>-1</sup>	$\frac{\partial\sigma}{\partial T}$ mN m <sup>-1</sup> K <sup>-1</sup>
Al	933	896	$-1.9 \times 10^{-4}$
Cu	1357	1339	$-1.8 \times 10^{-4}$
Au	1338	1162	$-1.8 \times 10^{-4}$
In	430	562	$-0.98 \times 10^{-4}$
Pb	601	450	$-0.86 \times 10^{-4}$
Ag	1234	9140	$-1.5 \times 10^{-4}$
Co	1768	1887	$-3.3 \times 10^{-4}$
Fe	1809	1870	$-4.3 \times 10^{-4}$
Ni	1728	1770	$-3.3 \times 10^{-4}$
Si	1638	784	$-6.5 \times 10^{-4}$

under these conditions have not been made, although it has been estimated Hara and Ogno to be 660 mN m<sup>-1</sup>.<sup>[58]</sup>

#### E. Surface Tension and Bonding

Molten oxides have significantly lower surface tension compared to their molten metal counterparts, in spite of the high melting temperature of the compounds.

The surface tension can be thought of as a measure of the strength of in-plane atomic Gibbs energy. This results in a drive to reduce the excess energy from unsatisfied bonds on the surface. The degree to which the directionality of atomic bonding changes can be linked to the ascribed character of the bond: metallic, covalent, and ionic.

Metallic bonding is recognized to have the least angular dependence. As such, metals should experience the least dramatic reduction in total cohesion due to the loss of outer plane bonding members. This reasoning is supported by the successful modeling of the energy of metallic systems as proportional to the square root of the number nearest neighbor atom count.<sup>[59-61]</sup>

However, the oxides examined in this work are ionic and covalent in bonding character. If one assumes pure ionic character, this is often modeled using a coulomb potential, resulting in a system energy which varies linearly with the number of nearest neighbors. This implies that ionic systems should experience a stronger drop in cohesion per atom removed, and therefore, weaker in plane bonding corresponding to a lower surface tension.

As one would expect, metallic elements have larger surface tension values compared to oxides; a brief survey of which is presented in Table V. Semi-empirical trends have been established for the surface tension of metals in relation to their molten molar volumes and melting temperatures given by the equation:

$$\sigma = \frac{kT_m}{V_m^{2/3}}, \quad [6]$$

where  $k$  is a constant that falls between 3.4 and 4 for elemental metals. Schytil was the first to propose such a relation with the factor  $\frac{kT_m}{V_m^{2/3}}$  representing an indirect

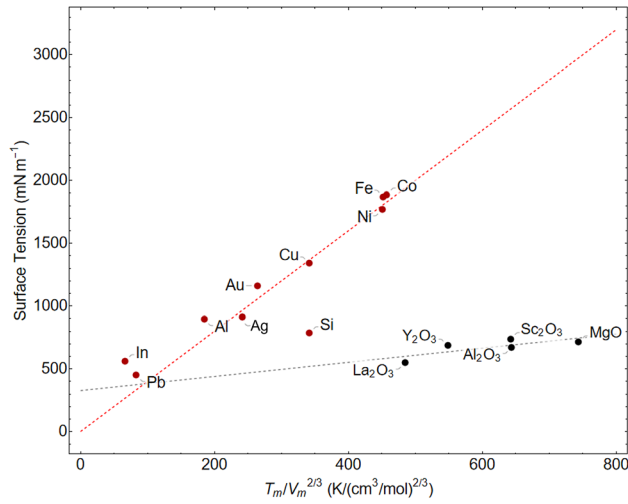


Fig. 9—Evaluation of the surface tension with the respect to the phenomenological model of Eq. [6].

characteristic of the binding energy in metals as reported by Kononenko *et al.*<sup>[62]</sup> It was demonstrated by Iida that the same relation could be reached using a simple harmonic oscillator model for atoms in the liquid.<sup>[63]</sup>

Using the surface tension values compiled in Table V, molten molar volumes from Lide, and our own data, we examine the validity of the relation in Eq. [6] for the surface tension of molten oxides.<sup>[64]</sup> The results are plotted in Figure 9.

The best-fit line in the case of the studied oxides results in a  $k = 0.56$ . It should be noted, however that this relationship has an offset, so that while some trend exists among the variation of the volume normalized melting temperature for these particular molten oxides, unlike elemental metals, Eq. [6] is not applicable for these materials. The molar volumes reported for the oxide elements are normalized to the average molar volume per atom to compare solutions with different stoichiometry. The success of such a simple relation implies that the melting temperature adequately captures the total bonding strength of the studied oxides, irrespective of the differences in ionic and covalent bonding character.

Interestingly, a reduction in the metallic character of the bond, even among pure elements, corresponds to a reduction in the surface tension (Si, In, and Pb) compared to transition metals (Fe, Ni).

#### F. Connection to the Enthalpy of Vaporization

The data were used to connect the surface tension values for oxides to the enthalpy of vaporization. A relation similar to Eq. [6] is often attributed to Skapski<sup>[66,67]</sup> as follows:

$$\sigma = \frac{k' \Delta H_v}{V_m^{2/3}}. \quad [7]$$

Table VI. Relevant Data for the Estimation of the Enthalpy of Vaporization for Various Oxides

Material	$\Delta H_{\text{fus}}$ kJ mol <sup>-1</sup>	Sources	$\Delta H_v$ MJ mol <sup>-1</sup>
Y <sub>2</sub> O <sub>3</sub>	84	[72]	2.67
Al <sub>2</sub> O <sub>3</sub>	112	[73]	2.22
MgO	77.8	[74]	0.67
Sc <sub>2</sub> O <sub>3</sub>	96.3	[75]	2.56
La <sub>2</sub> O <sub>3</sub>	78	[76]	2.14

Research by Tanaka *et al.* has already demonstrated the utility of this relationship for some molten oxides, and we refer the reader to additional discussion there.<sup>[18]</sup> If Eq. [7] proves to be a general relation, the enthalpy of vaporization can be reliably calculated from the surface tension, which would be significant considering the  $\Delta H_v$  is a quantity in which there are comparatively little data in the liquid state for oxides. The surface tension could be used as a fundamental probe of gaseous associate formation, as in the case of MgO which can either form gaseous Mg, O<sub>2</sub>, or MgO. We believe that gas-phase effects may be significant in this particular case because unlike the other oxides in this study, MgO was only stabilized under a large partial pressure of oxygen (3.5 atm), leading to the oxidation of the primary vaporized constituent. Because the vaporization enthalpies are widely unavailable for the oxides in this study, they were back-calculated from the enthalpies of sublimation and fusion. The enthalpy of sublimation was calculated according to

$$\Delta H_{\text{sub}} = -\Delta H_{\text{form}} + a\Delta H_{\text{at}} \quad [8]$$

for an oxide of stoichiometry M<sub>a</sub>O<sub>b</sub>. Here,  $\Delta H_{\text{at}}$  is the enthalpy of atomization of the metal and  $\Delta H_{\text{form}}$  is the standard state enthalpy of formation of gaseous oxygen and the metal.

Because of the availability of enthalpy of fusion data for the relevant oxides, the enthalpy of vaporization was calculated as the difference of the sublimation and fusion enthalpies:

$$\Delta H_v = \Delta H_{\text{sub}} - \Delta H_{\text{fus}} \quad [9]$$

Fusion enthalpies from the literature are listed in Table VI below. Atomization enthalpies for the rare-earth elements, Al, and Mg were taken from the references.<sup>[68,69]</sup> Formation enthalpies were also taken from Adachi *et al.* for the rare-earth oxides and Elliott and Gleiser for MgO and Mah for Al<sub>2</sub>O<sub>3</sub>.<sup>[70,71]</sup>

The resulting calculations for the enthalpy of vaporization are plotted with respect to Eq. [7] in Figure 10.

A weak linear trend is observed with the exclusion of MgO. It is believed that complex gaseous associate formation renders the gross assumptions in Eq. [8] invalid for MgO and any other similarly behaving oxides. However, this increases our confidence in the quality of the surface tension measurements for the remaining oxides. We believe that fundamental,

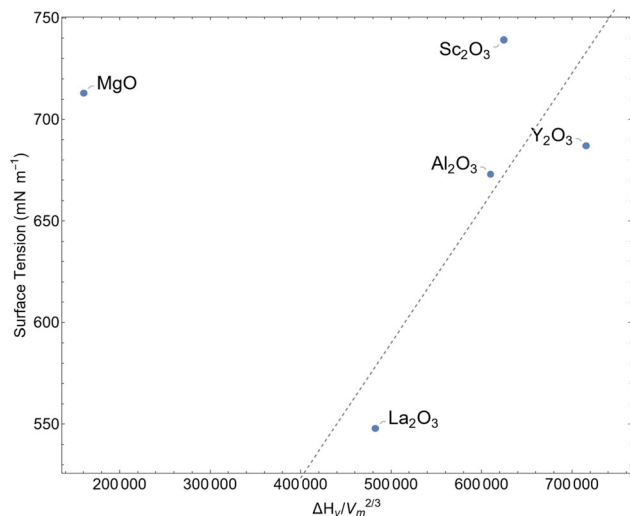


Fig. 10—Enthalpy of vaporization normalized by the molar volume vs. surface tension.

physically motivated relations exist that could tie surface tension measurements to the enthalpy of vaporization and would be a worthy goal for future research.

#### IV. CONCLUSIONS

The surface tension and molten density for  $\text{Al}_2\text{O}_3$ ,  $\text{Y}_2\text{O}_3$ ,  $\text{La}_2\text{O}_3$ ,  $\text{Sc}_2\text{O}_3$ , and  $\text{MgO}$  was measured using a thermal imaging furnace. The strength of the method has been confirmed, and the data agree with semi-empirical relations derived for the surface tension of molten metals. The surface tension and density of  $\text{MgO}$  and  $\text{Sc}_2\text{O}_3$  are reported upon for the first time.<sup>[14]</sup>

#### ACKNOWLEDGMENTS

The authors would like to acknowledge financial support for this project from both the National Science Foundation (NSF), under grant number 1562545 and the Air Force Office of Scientific Research under award number FA9550-20-1-0163. We would like to thank the Sumitomo Metal Mining Company for generously providing  $\text{Sc}_2\text{O}_3$ .

#### CONFLICT OF INTEREST

The authors declare that they have no conflict of interest.

#### FUNDING

Open Access funding provided by the MIT Libraries.

#### OPEN ACCESS

This article is licensed under a Creative Commons Attribution 4.0 International License, which permits use, sharing, adaptation, distribution and reproduction in any medium or format, as long as you give appropriate credit to the original author(s) and the source, provide a link to the Creative Commons licence, and indicate if changes were made. The images or other third party material in this article are included in the article's Creative Commons licence, unless indicated otherwise in a credit line to the material. If material is not included in the article's Creative Commons licence and your intended use is not permitted by statutory regulation or exceeds the permitted use, you will need to obtain permission directly from the copyright holder. To view a copy of this licence, visit <http://creativecommons.org/licenses/by/4.0/>.

#### REFERENCES

1. M. Gasik, V. Dashevskii, and A. Bizhanov, *Ferroalloys with Rare-Earth Metals*, Springer, Berlin, 2020.
2. P. Sahoo, T. DebRoy, and M. McNallan, *Metall. Trans. B*, 1988, vol. 19, pp. 483–91.
3. E.T. Turkdogan, *Physicochemical Properties of Molten Slags and Glasses*, Metals Society, London, 1983.
4. S. Bublik, J.E. Olsen, V. Loomba, Q.G. Reynolds, and K.E. Einarsrud, *Metall. Mater. Trans. B*, 2021, pp. 1–10.
5. D.J. Bradwell, H. Kim, A.H. Sirk, and D.R. Sadoway, *J. Am. Chem. Soc.*, 2012, vol. 134(4), pp. 1895–1897.
6. K. Wang, K. Jiang, B. Chung, T. Ouchi, P.J. Burke, D.A. Boysen, D.J. Bradwell, H. Kim, U. Muecke, and D.R. Sadoway, *Nature*, 2014, vol. 514(7522), pp. 348–50.
7. F.D. Richardson, *Physical Chemistry of Melts in Metallurgy*, Academic Press, London, 1974.
8. K. Mills, L. Yuan, and R. Jones, *J. South Afr. Inst. Min. Metall.*, 2011, vol. 111(10), pp. 649–58.
9. J.W. Gibbs, *The collected works of J. Willard Gibbs*. Technical Report, Yale University Press, 1948.
10. C.H. Lupis, *Chemical thermodynamics of materials*, 1983.
11. J.A.V. Butler, *Proc. R. Soc. Lond.*, 1932, vol. 135(827), pp. 348–75.
12. G. Kaptay, *Langmuir*, 2019, vol. 35(33), pp. 10987–92.
13. T. Tanaka, K. Hack, and S. Hara, *MRS Bull.*, 1999, vol. 24(4), pp. 45–51.
14. Materion, *Scandium Oxide  $\text{Sc}_2\text{O}_3$  for Optical Coating*. <https://materion.com/resource-center/product-data-andrelated-literature/inorganic-chemicals/oxides/scandium-oxidesc2o3-for-optical-coating>.
15. J. Hajra, and M. Divakar, *Metall. Mater. Trans. B.*, 1996, vol. 27, pp. 241–53.
16. J. Eberhart, *J. Phys. Chem.*, 1966, vol. 70(4), pp. 1183–86.
17. T. Tanaka, T. Kitamura, and I.A. Back, *ISIJ Int.*, 2006, vol. 46(3), pp. 400–06.
18. T. Tanaka, K. Hack, T. Iida, and S. Hara, *Z. Met.*, 1996, vol. 87(5), pp. 380–89.
19. S. Atlas, *Verlag Stahleisen GmbH, Düsseldorf*, 1995, vol. 111.
20. P. Bhattacharyya, and D. Gaskell, *Metall. Mater. Trans. B*, 1996, vol. 27, pp. 139–41.
21. S. Fordham, *Proc. R. Soc. Lond. A*, 1948, vol. 194(1036), pp. 1–16.
22. W.D. Kingery, *J. Am. Ceram. Soc.*, 1959, vol. 42(1), pp. 6–10.
23. A.D. Kirshenbaum, and J.A. Cahill, *J. Inorg. Nucl. Chem.*, 1960, vol. 14(3–4), pp. 283–87.
24. M.A. Maurakh, B.S. Mitin, and M.B. Roitberg, *Zavod. Lab.*, 1967, vol. 33(8), pp. 984–85.
25. Y.V. Zubarev, V.I. Kostikov, B.S. Mitin, Y.A. Nagibin, and V.V. Nishcheta, *Izv. Akad. Nauk SSSR Neorg. Mater.*, 1969, vol. 5(9), pp. 1563–65.

26. V. Elyutin, B. Mitin, and Y. Nagbin, *Zavod. Lab.*, 1971, vol. 37(2), p. 246.
27. J.J. Rasmussen, and R.P. Nelson, *J. Am. Ceram. Soc.*, 1971, vol. 54(8), pp. 398–401.
28. B. Mitin, and Y.A. Nagbin, *Russ. J. Phys. Chem. USSR*, 1970, vol. 44(5), p. 741.
29. N. Ikemiya, J. Umemoto, S. Hara, and K. Ogino, *ISIJ Int.*, 1993, vol. 33(1), pp. 156–65.
30. H. Von Wartenberg, G. Wehner, and E. Saran, *Nachr. Ges. Wiss. Göttingen, Math.-physik. Klasse. Fachgruppe II [NF]*, 1936, vol. 2, pp. 65–71.
31. R. Bartlett, and J. Hall, *Am. Ceram. Soc. Bull.*, 1965, vol. 44(5), p. 444.
32. R.N. McNally, H.C. Yeh, and N. Balasubramanian, *J. Mater. Sci.*, 1968, vol. 3(2), pp. 136–38.
33. J.M. Lihmann, and J.S. Haggerty, *J. Am. Ceram. Soc.*, 1985, vol. 68(2), pp. 81–85.
34. M. Zhu, G. Wu, A. Azarov, E. Monakhov, K. Tang, M. Müller, and J. Safarian, *Metall. Mater. Trans. B*, 2021, pp. 1–19.
35. M. Gan, Z. Dan, S. Zhang, Q. Wang, X. Zhang, S. He, and Q. Wang, *Metall. Mater. Trans. B.*, 2020, vol. 51(2), pp. 677–89.
36. B. Granier, and S. Heurtault, *J. Am. Ceram. Soc.*, 1988, vol. 71(11), pp. C466–68.
37. E. Savitsky and V. Terekhova, in *Colloq. Int. CNRS*, vol. 180, pp. 47–60.
38. T. Massalski, H. Okamoto, and P. Subramanian, *ASM Int.*, 1990, vol. 2 (2882).
39. E. Shpilrain, D. Kagan, L. Barkhatov, V. Koroleva, J. Coutures, and M. Foex, *Colloque International (1977)*.
40. S. Schneider, and J. Waring, *J. Res. Natl. Bureau Std. Sect. A*, 1963, vol. 67A(1), p. 19.
41. T. Noguchi, and M. Mizuno, *Sol. Energy*, 1967, vol. 11(2), pp. 90–94.
42. J.P. Coutures, R. Verges, and M. Foex, *Rev. Int. Hautes Temp. Refract.*, 1975, vol. 12(2), pp. 181–85.
43. H. Cong, H. Zhang, B. Yao, W. Yu, X. Zhao, J. Wang, and G. Zhang, *Cryst. Growth Des.*, 2010, vol. 10, pp. 4389–4400.
44. A. Bartos, K.P. Lieb, M. Uhrmacher, and D. Wiarda, *Acta Crystallogr. B*, 1993, vol. 49(2), pp. 165–69.
45. T. Schleid, and G. Meyer, *J. Less-Common Met.*, 1989, vol. 149, pp. 73–80.
46. R.N. Kemi, *Arkiv for Kemi*, 1968, vol. 29 (4).
47. O. Knop, and J.M. Hartley, *Can. J. Chem.*, 1968, vol. 46(8), pp. 1446–1450.
48. S. Geller, P. Romo, and J.P. Remeika, *Zeitschrift für Kristallographie - New Cryst. Struct.*, 1967, vol. 124(1–2), 136–142.
49. A. Men'kov, L. Komissarova, Y.P. Simanov, and V.I. Spitsyn, *Dokl. Akad. Nauk SSSR*, 1961, vol. 141(2), pp. 364–67.
50. D.W. Stacy, *Thermal expansion of the sesquioxides of yttrium, scandium, and gadolinium*, Digital Repository@ Iowa State University, <http://lib.dr.iastate.edu/> (1967).
51. N. José, H. Ahmed, B. Miguel, E. Luís, and D.B. Jorge et al., *Materials*. 2020, vol. 13(21), p. 4752.
52. B.R. Nakanishi, and A. Allanore, *J. Electrochem. Soc.*, 2017, vol. 164(13), pp. E460–71.
53. M. Wu, A.H. Caldwell, and A. Allanore, in *Minerals* (Springer International Publishing, Metals and Materials Series, 2019), pp. 33–41.
54. Omega type c thermocouple reference, Tech. rep.
55. J.D. Berry, M.J. Neeson, R.R. Dagastine, D.Y. Chan, and R.F. Tabor, *J. Colloid Interface Sci.*, 2015, vol. 454, pp. 226–37.
56. H. Okamoto, and T.B. Massalski, *J. Phase Equilib.*, 1994, vol. 15(5), pp. 500–21.
57. V.I. Kohonenko, A.L. Sukhman, S.L. Gruverman, and V.V. Torokin, *Phys. Status Solidi (a)*, 1984, vol. 84(2), pp. 423–32.
58. S. Hara, and K. Ogino, *Nippon Kinzoku Gakkai-si*, 1988, vol. 52(11), pp. 1098–1102.
59. M.W. Finnis, and J.E. Sinclair, *Philos. Mag. A*, 1984, vol. 50(1), pp. 45–55.
60. F. Ercolessi, M. Parrinello, and E. Tosatti, *Philos. Mag. A*, 1988, vol. 58(1), pp. 213–26.
61. S. Nishitani, P. Alinaghian, C. Hausleitner, and D. Pettifor, *Philos. Mag. Lett.*, 1994, vol. 69(4), pp. 177–84.
62. V.I. Kononenko, A.L. Sukhman, S.L. Gruverman, and V.V. Torokin, *Phys. Status Solidi (a)*, 1984, vol. 84(2), pp. 423–32.
63. T. Iida, R. Guthrie, *The Thermophysical Properties of Metallic Liquids: Fundamentals*, Oxford University Press, Oxford, 2015.
64. D. Lide, *CRC Handbook of Chemistry and Physics*, CRC Press, Philadelphia, 2004.
65. I. Egry, E. Ricci, R. Novakovic, and S. Ozawa, *Surface tension of liquid metals and alloys-Recent developments* (2010).
66. A.S. Skapski, *Acta Metall.*, 1956, vol. 4(6), pp. 576–82.
67. A.S. Skapski, *J. Chem. Phys.*, 1948, vol. 16(4), pp. 389–93.
68. G.Y. Adachi, and N. Imanaka, *Chem. Rev.*, 1998, vol. 98(4), pp. 1479–1514.
69. H. Heinz, and U.W. Suter, *J. Phys. Chem. B*, 2004, vol. 108(47), pp. 18341–352.
70. A.M. Poston, A.D. Mah, A.R. Taylor, C. Zahn, D. Bienstock, D.F. Smith, F. Wideman, H.F. Yancey, J.M. Riley, L. Obert et al., *Heats and Free Energies of Formation of Gallium Sesquioxide and Scandium Sesquioxide, 5961–5980*. US Department of the Interior, Bureau of Mines, 1962.
71. J.F. Elliott, M. Gleiser, and V. Ramakrishna, *Thermochemistry for Steelmaking*, vol. 2, Pergamon, London, 1963.
72. E.E. Shpilrain, D.N. Kagan, L.S. Barkhatov, V.V. Koroleva, J.P. Coutures, and M. Foex, *Rev. Int. Hautes Temp. Refract.*, 1978, vol. 15(3), pp. 249–52.
73. D. Jerebtsov, and G. Mikhailov, *Ceram. Int.*, 2001, vol. 27(1), pp. 25–28.
74. M.W. Chase, J.L. Curnutt, R.A. McDonald, and A.N. Syverud, *J. Phys. Chem. Ref. Data*, 1978, vol. 7(3), pp. 793–940.
75. G.V. Samsonov, *The Oxide Handbook*, IFI/Plenum, New York, 1982.
76. S.V. Ushakov, and A. Navrotsky, *J. Mater. Res.*, 2011, vol. 26(7), pp. 845–47.

**Publisher's Note** Springer Nature remains neutral with regard to jurisdictional claims in published maps and institutional affiliations.